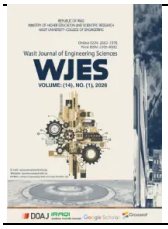

Wasit Journal of Engineering Sciences
Journal homepage: https://ejuow.uowasit.edu.iq

ISSN 2305-6932
Original Research

Vol. 14 No. 1 March 2026, pp.1-14
https://doi.org/10.31185/ejuow.v14i1.645

Estimating the Solar Fraction of a Closed Solar Water Heating System Using the Utilizability F-Chart Method under Various Operating Conditions

Fatima Hilal Abish[1], Abdulsalam D. M. Hassen[1]
[1] Department of Mechanical Engineering, College of Engineering, Wasit University, Wasit, Iraq

Corresponding Author Email:Std2022203.F.HI@uowasit.edu.iq

Received Feb.23, 2025 | Revised Jul.17, 2025 | Accepted Aug.29, 2025 | Online March.1, 2026

ABSTRACT

The increasing demand for sustainable cooling technologies and the shift away from fossil fuels have heightened interest in solar-assisted thermal systems, particularly for powering absorption refrigeration units in hot environments. This study evaluated the performance of a closed-loop solar water heating system used to supply hot water to an absorption refrigeration machine. The analysis was carried out using the utilizability (f-chart) method and the MATHLAP computer program. The study considered various operating conditions and four types of flat-plate solar collectors: Type A: Single transparent cover solar collector with absorbent surface painted in standard black color; Type B: Single transparent cover solar collector with absorbent surface coated in black selective material; Type C: Solar collector with two transparent covers with absorbent surface painted in standard black color; and Type D: Solar collector with two transparent covers with absorbent surface coated in black selective material. The system was analyzed for different solar collector areas and storage capacities over several summer months. The solar fraction (f) was used as the primary performance metric. The results indicated that Type D collectors performed the best owing to their improved thermal insulation and selective absorption. Type A exhibited the lowest performance because of its higher heat losses. Types B and C yielded intermediate results. The study also examined the effect of five storage capacities (25, 50, 75, 100, and 125 kg of water per m²) and five collector areas (40, 60, 80, 100, and 120 m²) on system efficiency. Both parameters positively affected the thermal performance. This study aims to determine the thermal performance of a closed-loop solar water heating system for powering an absorption refrigeration machine by estimating the solar fraction under different conditions.

Keywords: Solar water heating system, Thermal performance, Solar collector, Solar fraction, Storage capacity, Solar collection area.

1. Introduction

As energy needs rise, fuel prices soar, and concerns for our environment fluctuate, solar water heating systems have emerged as a sustainable alternative to conventional water heating systems. Solar water heating systems harness solar energy to meet domestic or industrial hot water needs, which are clean, affordable, and reduce dependence on fossil fuels [1]. Of the many different types of solar water heating systems, closed-loop systems have become very popular in colder regions because they do not freeze and are capable of maintaining a functional system in harsh winters. The solar fraction (SF) is a key parameter for quantifying the overall performance of solar water heating systems, referring to the overall thermal load contributed by solar energy. A higher solar fraction indicates greater potential for energy savings and environmental benefits [2]. However, performance is influenced by many factors, such as collector efficiency, climate conditions, heat exchanger effectiveness, and system design. This study is based on closed-loop solar water heating systems and explores the system efficiency based on the solar fraction as a performance target. The objective is to identify configurations and operational strategies to maximize energy savings and system reliability via thermal analysis, modelling methods, and performance evaluation under different constraints [3].

1.1. The “f-chart” method

Fayaz et al.[4] the study assesses the performance of evacuated tube solar water heaters employing the F-chart method as a benign technology. This demonstrates how well and economically it performs in the Malaysian climate. The system can deliver 150 liters of hot water daily without an auxiliary energy supply and a solar fraction of 1.0. An evacuated tube channel will cost RM 5,200 over 20 years, and if used in climates with consumption exceeding 150 L/d, it can save up to RM 12,000. The study suggests that the benefits are also environmental; reductions in GHG gas emissions are substantial, along with energy use. Hence, an evacuated tube solar water heater is a sustainable choice.

Kerme and Kaneesamkandi,[5] primarily focused on the development of a liquid-based solar heating system using the F-chart method, which is an efficient and cost-effective method for estimating annual thermal performance. They considered the contribution of solar energy to the heating loads for a family of six people living in Riyadh, Saudi Arabia, and examined parameters such as collector area, storage capacity, and tilt angle. The f-chart method allows a relationship between the monthly heating load supplied by solar energy and dimensionless parameters, allowing for a simpler estimation of performance. The results suggest that by increasing the collector area, the annual load fraction supplied by solar energy improved, particularly in the summer months. The best tilt angle for collectors in Riyadh was 30 °, according to the analysis in the study, which allowed the solar load fraction to be maximized. The study determined that the effect of storage capacity on performance was greater in summer than in winter.

Çamdali and Tunç,[6] the paper applies the F-Chart method to optimally size solar collectors and storage capacity, indicating that a solar fraction of 92% can meet the total energy demand for space and water heating in Cesme, Turkey. Solar radiation of 1304 kWh/m²-year was measured for 2734 h/year over a period of 2 years. Considering the space heating and hot water demand in this geographic area, the solar collector and storage capacity were sized optimally using the f-chart method.

Gojak et al.,[7] The paper describes the calculation of the solar fraction, i.e., the contribution of solar energy to the total heat load, using a mathematical model, with the results of the simulations compared to the results of the f-chart method, and given the performance of the system for the city of Belgrade in Serbia. The authors built a dynamic simulation model to build a thermal solar system concerned with the energy performance for water heating. Their model considered the variability of factors such as climatic data, hot water consumption dynamics, system parts, dynamics within the fluid flow, and the orientation of the solar collector to optimize solar system operation. El-Masri et al. [8] El-Masri et al. effectively utilized the f-chart method, emphasizing its reliability when paired with local radiation data. These models estimate the efficiency of solar heating systems in terms of heat, using precise physical equations. Although computationally expensive and requiring significant input data, they provide accurate results [9]. Hoffmann et al. [10] discuss the challenges associated with the f-chart method for closed-loop systems utilizing antifreeze fluids in regions such as Northern Europe are discussed. To enhance the accuracy of the solar fraction calculations under freezing conditions, the loss coefficient (U) was modified to account for the thermal properties of the antifreeze. The f-chart method must also be adapted to reflect the increasing prevalence of systems integrating solar thermal and photovoltaic power sources [11]. Fong et al.[12] the f-chart method was employed in their research on solar-assisted heat pump systems. Their findings indicated that both residential and commercial systems performed better when the dimensionless parameters (X and Y) were adjusted to account for the combined heat contributions of solar and heat pump systems. Sangeetha et al. [13] explored ways to improve the accuracy of solar fraction estimates by integrating the f-chart method with machine learning techniques. This was achieved by significantly reducing the error margin during model training using large volumes of simulated data. Recent updates to the f-chart method have incorporated real-time weather data, enhancing the adaptability of the tool to various climates [14]. Wu et al.[15] a two-dimensional model of the Trombe wall's thermal efficiency and air purification capabilities was numerically investigated. The relationships between the diffusion and convection and free convection heat transfer equations were used to solve several physical fields. The numerical results were closely aligned with the experimental data found in the relevant literature. Environmental factors, operational conditions, and geometric structures influenced the rate at which the Trombe wall degraded formaldehyde and its thermal performance. The findings demonstrated that the thermal efficiency decreased as the ambient temperature and solar radiation increased; conversely, higher air inlet temperatures and ambient wind velocities improved performance. Notably, the thermal performance increased initially but then declined as the channel width increased, with a maximum thermal efficiency of 53% reached at a width of 0.04 m. A distinct pattern of increasing and subsequently decreasing air purification rates was observed across all variables. Si et al. [16]

proposed an innovative envelope connecting passive solar buildings with variable thermal performance. Field tests validated the practicality of establishing an ideal indoor environment, particularly in cold plateau regions, by combining a transparent building envelope with a step-operation control technique. The results from these trials indicated that the proposed building envelope effectively enhanced heat gain and maintained a comfortable indoor temperature, even in extreme weather conditions. The highest recorded room temperature during the investigation was 21 degrees Celsius, while the average temperatures ranged between 13.5 and 14.0 degrees Celsius.

Al-Maliki and Al-Nadawi [17] noted that solar thermal energy has become essential as advancements in building construction engineering and natural energy sources continue. This study investigates the long-term thermal performance of an absorber-storage wall system using the Utilizability, f-chat approach (generic design). MATHLAP was employed to solve the mathematical model equations related to thermal performance and to calculate the system's solar fraction factor (f) for the four winter months of November to February, utilizing daily weather data from Kut city based on monthly averages. This analysis revealed that increasing the wall area and decreasing the wall thickness improved the solar fraction factor. Among different materials, concrete outperformed bricks and stones, achieving a maximum solar percentage factor of 94.16% in November with a wall size of 60 m² and a thickness of 10 cm. Additionally, the study found that the average solar fraction factor for the passive heating system was 0.7. Solar energy could cover up to 70% of room heating needs, depending on the climate. Alayi et al., [18] in this article, a system designed in this research is presented that can satisfy 75% of the hot water use rate, and if an auxiliary heat source is utilized alongside this system, this will satisfy the entire hot water needs of the building year-round. Juan et al. [19] noted that solar thermal systems are increasingly recognized as a viable option for generating heat for industrial processes in the context of a push for zero-carbon energy. This technology is employed in various applications; however, no consensus exists on the best methods for scaling or controlling these systems. The variability of solar energy and the fluctuating thermal demands of industries necessitate specific design strategies. Huang et al.,[20] this work outlined the reforms were applied to the hot water supply system. The operational strategy was modified as well. The other apartment remained unchanged. The energy consumption, solar fraction, water supply quality, and economics of the two systems were analyzed and compared. The results indicated that the transformation plan is reasonable and feasible. The solar fraction had a significant improvement in the transformed system. The original system water supply temperature fluctuated from 35 °C to 60 °C, but it was shown to stabilize between 40 °C and 50 °C after the transformations. The average power saving rate of the transformed system reached 72.70%, and this economic benefit is very good. Moreover, the TRNSYS simulation software was used to model and optimize the control of the system.

1.2. The utilizability method ($\bar{\phi}$)

The utilizability method ($\bar{\phi}$) used for designing solar systems computes the thermal performance of solar systems over time using traditional flat-plate collectors. Whillier proposed this in 1953 [21]. The fundamental basis of this method, known as the ϕ-curve method, is examining hourly meteorological data. The required computations are executed hourly, once a month, at solar noon. Liu and Jordan [22] Further, the seasonal and geographical elements technique was developed. With this expansion created from daily data, building usability curves at any position and tilt is feasible using the clarity index (KT). Zlateva,[23]In this paper the long-term performance of flat-plate and evacuated tube solar collectors operating under varying conditions will be assessed. The analysis will include the calculation of the daily utilizability factor, which is defined as the ratio of total monthly solar radiation over an inclined surface to the critical value, and Collares-Pereira and Rabl [24]. Calculations must be performed hourly. This method significantly improved benefits while decreasing complexity, as seen by the monthly average daily usage.

1.3. The" $\bar{\phi}$f-chart design" technique for solar power systems with closed-loop systems

Researchers Klein and Beckman [25] Developed a method that combines the f-chart technique with the Utilization principle, offering an alternative approach to system development. The closed-loop system illustrated in Fig. 1 represents one possible way to integrate this technology into a solar energy system. It is important to note the assumptions made to depict the solar system in Fig. 1. The" $\bar{\phi}$f-chart design" technique for solar power systems with closed-loop systems. First, the storage tank must be filled with a highly vaporizing liquid or pressurized accordingly. An auxiliary heater must be installed parallel to the solar system. The energy supplied to the load region must reach a temperature equal to or greater than a specified minimum applicable temperature (Tmin).

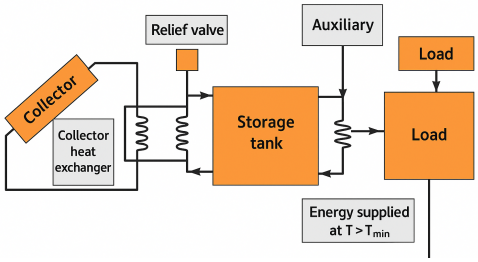

Figure 1. Solar Energy System Schematic Depicting a Closed-Loop Configuration [26]

2. Mathematical analysis

2.1. Utilizability concept

The utlizability can be directly determined using the "Hottel-Whillier-Bliss" equation, as in Eq. (1), which is a function of the hourly "solar radiation" (Ht) and the concentrator's transmissivity-absorptivity product (τα) [27].

$$Q_u = A_C F_R[H_t(\tau\alpha) - U_C(T_i - T_a)] \quad (1)$$

As shown in the previous equation, a particular quantity of radiation is needed to raise the collector's absorbing surface temperature to the same level as the fluid's inlet temperature. Putting the value of Qu to zero in Eq. (1) yields this minimal radiation level, abbreviated as (Ht,c), which is also known as the critical level which is illustrated in Eq. (2):

$$H_{t,c} = \left[\frac{F_R U_c(T_i - T_a)}{F_R(\tau\alpha)}\right] \quad (2)$$

The amount of incident solar radiation must exceed a critical threshold for the solar collector to produce usable energy. Modify the equation accordingly by substituting Eq. (2) into Eq. (1) gives the following relationship:

$$Q_u = A_C F_R(\tau\alpha)\left(H_t - H_{t,c}\right) \quad (3)$$

The useful hourly energy shown in Eq. (4) collected at a specific hour of a specific day and calculated on an average basis over a long period (usually a month) of N days can be written as follows [25] [28]:

$$\overline{Q'_u} = \frac{A_C F_R(\tau\alpha)}{N} \sum_N \left(H_t - H_{t,c}\right) \quad (4)$$

Assume that $\overline{H'_t}$represents the average monthly value of hourly solar radiation at a particular hour of a specific day. Therefore, the hourly utlizability Φ will be a fraction or part of the amount $\overline{H'_t}$ with a level higher than the critical level $H_{t,c}$, and thus shown in Eq. (5):

$$\emptyset = \frac{1}{N} \sum_N \frac{(H_t - H_{t,c})}{\overline{H'_t}} \quad (5)$$

As an example of the average monthly value of collected useful energy for a specific hour of the day, one can write it as [19]:

$$\overline{Q'_u} = A_C F_R(\tau\alpha)\overline{H'_t}\emptyset \quad (6)$$

The product of the total daily radiation incident on the tilted solar collector $\overline{R} * \overline{H}$ and ($\overline{H_t}$) can be utilized to simplify the utilizability computation. Thus, the average utilizability per month ($\overline{\emptyset}$) is the percentage of total solar radiation during a month with N days, which is more than the critical level as in Eq. (7):

$$\overline{\emptyset} = \sum_{days} \sum_{hours} \frac{(H_t - H_{t,c})}{\overline{H_t}\, N} \quad (7)$$

The critical level can be redefined in terms of the monthly average values of transmissivity-absorptivity product ($\overline{\tau\alpha}$) and ambient temperature during daylight hours ($\overline{T_a}$) as illustrated in Eq. (8):

$$H_{t,c} = \frac{F_R U_c(T_i - \overline{T_a})}{F_R(\overline{\tau\alpha})} \quad (8)$$

The following relationship can give the "monthly average" of the accumulated daily useful energy:

$$\overline{Q_u} = \mathrm{A_C} F_R (\overline{\tau\alpha}) \overline{H_t} \overline{\varphi} \quad (9)$$

According to the following relationship ($\bar{\phi}$) the monthly clearness index ($\bar{\mathrm{K}}_\mathrm{T}$) plus two other variables, the geometry factor $\left(\frac{\mathrm{R_n}}{\bar{\mathrm{R}}}\right)$ and the lowest value of the monthly average critical radiation ratio ($\bar{\mathrm{X}}_\mathrm{c}$), may completely characterize the value of ($\bar{\phi}$) [29] [30].

$$\bar{\phi} = e^{[A+B\left(\frac{R_n}{R}\right)\left(\overline{X_C}+C\overline{X_C}^2\right)]} \quad (10)$$

$$A = 7.10 - 20.00\bar{K}_T + 12.08(\bar{K}_T)^2$$

Where: $B = -8.02 + 18.16\bar{K}_T - 10.68(\bar{K}_T)^2$

$$C = -1.02 + 4.10\bar{K}_T - 1.96(\bar{K}_T)^2$$

$\bar{\mathrm{R}}$, in the given equation, is the monthly average total radiation tilt factor, which is the ratio of the total solar radiation falling on the collector's tilted surface to the total solar radiation falling on the horizontal plane.

$$\bar{R} = \frac{\overline{H_t}}{\bar{H}} = \left(1 - \frac{\overline{H_d}}{\bar{H}}\right)\overline{R_B} + \frac{\overline{H_d}}{\bar{H}}\left(\frac{1+cos\ S}{2}\right) + \rho_g\left(\frac{1-cos\ S}{2}\right) \quad (11)$$

$\frac{\bar{H}_d}{\bar{H}}$: Monthly average daily diffuse-to-total radiation ratio

$$\frac{\bar{H}_d}{\bar{H}} = 1.391 - 3.560\bar{K}_T + 4.189(\bar{K}_T)^2 - 2.137\ (\bar{K}_T)^3 \quad (12)$$

$$\bar{K}_T = \frac{\bar{H}}{\bar{H}_o}$$

ρ_g : ground reflectance, if there is no snow on the ground, ρ_g = 0.2 [24]

$$\bar{R}_B = \frac{cos(L-S)\ cos\ \delta\ sin\ \acute{h_s} + \frac{\pi}{180}\acute{h_s}\ sin(L-S)\ sin\ \delta}{cos\ L cos\ \delta\ sin\ h_s + \frac{\pi}{180}h_s\ sin\ L sin\ \delta} \quad (13)$$

h_S: Sunset hour angle on a horizontal surface

$$h_s = \cos^{-1}(-\tan\ L \cdot \tan\ \delta) \quad (14)$$

$\acute{h_s}$: Sunset hour angle on a tilted surface

$$\acute{h_s} = \min(h_s, \cos^{-1}(-\tan(L-S)\cdot\tan\delta)) \quad (15)$$

Where S is the surface tilt angle, L is the latitude angle of the location on the earth, and δ is the solar declination angle.

R_n in Eq. (10) represents the ratio between the total solar radiation at noon falling on a tilted surface to the total radiation at noon falling on the horizontal plane calculated based on the monthly average. It can be expressed by:

$$R_n = \left(1 - \frac{r_{dn}}{r_n}\cdot\frac{\overline{H_d}}{\bar{H}}\right)R_{B,n} + \left(\frac{r_{dn}}{r_n}\cdot\frac{\overline{H_d}}{\bar{H}}\right)\left(\frac{1+\cos\ S}{2}\right) + \rho_\mathrm{g}\left(\frac{1-\cos S}{2}\right) \quad (16)$$

The ratio of total radiation at noon to daily total radiation is denoted as ($\mathrm{r_{dn}}$) in this context, and the ratio of diffuse radiation at noon to daily diffuse radiation is denoted as ($\mathrm{r_n}$). At solar noon, the angle h = 0 can be expressed as the hourly value of, so:

$$\mathrm{r_{dn}} = \frac{\pi}{24} \times \left(\frac{1-\cos\ (h_s)}{\sin\ (h_s) - \left(\frac{\pi}{180}\right)\times h_s \times \cos\ (h_s)}\right) \quad (17)$$

$$r_n = r_{d\cdot n}\left(1.07 + 0.025\ \sin\ (h_s - 60)\right)$$

$\mathrm{R_{Bn}}$ Eq. (16) represents the ratio of noon beam radiation on a horizontal surface to that on a slanted surface:

$$R_{Bn} = \frac{\cos(\mathrm{L}-S)\cos\delta + \sin(L-S)\sin\delta}{\cos\mathrm{L}\cos\delta + \sin\mathrm{L}\sin\delta} \quad (18)$$

This equation states that the critical radiation ratio ($\bar{\mathrm{X}}_\mathrm{C}$) should be averaged monthly and is the ratio of the radiation at noon to the critical level. On a typical day of the month, this ratio should equal the total radiation for the day. Another way to put it is:

$$\bar{X}_C = \frac{H_{t,c}}{r_n R_n \bar{H}} \quad (19)$$

Or

$$\bar{X}_C = \frac{1}{r_n R_n \bar{K}_T \bar{H}_o}\left[\frac{F_R U_C (T_i - \bar{T}_a)}{F_R(\overline{\tau\alpha})}\right] \quad (20)$$

2.2. The $\bar{\phi}$ f-chart design method for closed-loop solar energy system

Merging these two design approaches created a hybrid of the utilizability and f-chart methods proposed by [31]. According to the $\bar{\phi}$ f-chart method for enclosed solar energy systems, such as the one depicted in Fig. 1, the energy delivered to the load must exceed a practical minimum temperature. In contrast, the temperature of this energy should not impact the system's efficiency [32] . The $\bar{\phi}$ f-chart design approach achieves its peak performance when the inlet temperature of the collector fluid is set at $T_{mim.}$. according to Eq. (8), the crucial radiation level will thus be:

$$H_{t,c\,min} = \left[\frac{F_R U_c (T_{mim.} - \bar{T}_a)}{F_R(\overline{\tau\alpha})}\right] \quad (21)$$

By analogy with Eq. (9), the maximum collected solar energy can be written as:

$$Q_{\max} = A_C\, F_R(\overline{\tau\alpha})\bar{H}_t N \bar{\emptyset}_{\max} \quad (22)$$

The maximum monthly average daily utilizability, denoted as $\bar{\emptyset}_{\max}$, can be determined using Eq. (10) and the minimal critical radiation ratio, denoted as ($\bar{X}_c$, min) as given by Eq. (23), where N is the number of days in the month.

$$\bar{X}_{c,\,\text{mim.}} = \frac{1}{r_n R_n \bar{H}}\left[\frac{F_R U_c (T'_{mim.} - \bar{T}_a)}{F_R(\overline{\tau\alpha})}\right] \quad (23)$$

It is noted that the useful minimum temperature $T_{mim.}$ has been placarded in the above equation by the effective minimum temperature $T'_{mim.}$ in order to deal with the low efficiency of the load heat exchanger in closed-loop systems. To adapt the solar fraction (f) to the monthly load energy (D), the effective minimum temperature can be defined by:

$$f = \frac{C_L (T'_{\text{mim}} - T_{\text{mim}})}{D} \quad (24)$$

For closed-loop systems

$$C_L = \in \quad (25)$$

$$C_{mim} = \in (\dot{m}\, C_P)_{mim} \quad (26)$$

The product of the load heat exchanger efficiency and the minimum monthly heat capacity rate across the heat exchanger. How the maximum monthly gathered energy ($Q_{max.}$) compares to the actual monthly collected energy (Q_u) is established according to the simulation results in the $\bar{\phi}$ f-chart design approach.

$$Q_u = Q_{max} - a \times \left(e^{bf} - 1\right) \times (1 - e^{cX}) \times \left(e^{dZ}\right) \times D \quad (27)$$

Where:

a= 0.015 (Ms C_P /350)$^{-0.76}$

b= 3.85 , c = - 0.15 , d = - 1.959

$$X = A_C\, \grave{F}_R U_C\ (100\ ℃)\ (\Delta t/D) \quad (28)$$

Z=D/C_L (100 ℃)

Storage tank energy loss is dealt with in the $\bar{\emptyset}, f - chart$ method by a T_s that satisfies the energy balance equation

$$fD = Q_u - (UA)_s (T_s - T_{\text{env}})\Delta t \quad (29)$$

The monthly average storage temperature T_s for energy loss calculation as defined in Eq. (28) is correlated with the effective minimum useful temperature T'_{mim}prime in the following expression. Here is a formula that correlates the monthly average storage temperature T_s for energy loss calculation with the effective minimum usable temperature T'_{mim} prime), as specified in Eq. (29).

$$T_s = T'_{\text{mim}} + g\left[e^{kf} - 1\right]e^{hZ} \quad (30)$$

Where:

g = (0.2136℃)(Ms C_P /350)$^{-0.704}$, h=-4.002 , k=4.702

Applying the $\overline{\emptyset}$, f-chart method in designing solar water heating systems necessitated an iterative solution for determining the effective minimum useful temperature and, consequently, the solar fraction factor (f).

2.3. Solar system performance analysis

The performance of the closed loop solar system Fig. (1), which can be used as one of its applications for supplying thermal energy (hot water) needed to operate the generator of an absorption chiller that can be connected to the system, has been studied in this research using the $\overline{\emptyset}$, f- chart method to calculate the solar fraction factor (solar contribution) of the system. The solar fraction factor values of the system have been calculated on a monthly basis for each of the summer months during which the system can operate, which are the months (5, 6 ,7 ,8 ,9). The calculations were carried out on a geographical location (Baghdad city/Iraq) at latitude 33.32^{o} N on different solar collection areas and on various types of solar collectors by building a computer program (MATHLAP) to carry out these calculations according to the assumptions and operating conditions listed below:

- The thermal energy required to be supplied to the generator of the absorption chiller is 25 kW for 10 hours per day at a minimum temperature of 80℃ during the summer months when the system can operate.
- The solar system is located in Baghdad City/IRAQ at latitude L = 33.32° N. The flat-plate collectors are oriented south at a tilt angle of S =23.32°.The angle was chosen is approximately the latitude of Baghdad, which is roughly 33.3°. However, many solar applications will use a tilt angle of (latitude - 10°) to optimize for performance in the summer months. A tilt angle of 23.32° was chosen based on [5].
- The value of the ratio $\overline{\tau\alpha}/(\tau\alpha)_n$, is 0.96 for the solar collector with one transparent cover and 0.94 for the solar collector with two transparent covers [27,33].
- The value of the ratio F'_R/F_R which represents a measure of the thermal performance penalty that must be paid due to using a heat exchanger in the collection loop, is equal to 0.96 [34].
- load heat exchanger effectiveness value $\in_L = 0.72$,with a minimum heat capacity of the fluid in this exchanger$(\dot{m}\, C_P)_{mim}$ =3400 W/K.
- overall heat losses coefficient of storage tank value $(UA)_s = 6\ W/K$,with a temperature of the storage tank environment $T_{env} = 24℃$.
- Table 1 lists solar radiation data and climatic conditions for the geographical location (Baghdad city).

Table 1. Climatic Conditions for Baghdad City (Iraq) Latitude 33.32°N

Month	$\overline{T}_a$ ℃	$\overline{H}$ MJ/m^2.day	$\overline{K}_T$
May	29.028	24.957	0.624
June	32.001	25.409	0.627
July	36.485	25.976	0.650
August	35.858	24.397	0.660
September	31.463	21.404	0.700

N.B: The average values of the coefficients ($\overline{T}_a$), ($\overline{H}$) and ($\overline{K}_T$) were determined using the daily readings over five years, values collected from weather stations linked to "the Iraqi Ministry of Agriculture."

- During the research, four types of solar collectors were used:

1. Type A: Single transparent cover solar collector with absorbent surface painted in standard black color.
2. Type B: Single transparent cover solar collector with absorbent surface coated in black selective material.
3. Type C: Solar collector with two transparent covers with an absorbent surface painted in standard black color.
4. Type D: Solar collector with two transparent covers with an absorbent surface coated with black selective material.

Table 2. Comparison of the Four Types of Solar Collectors

Collector Type	Number of Transparent Covers	Absorber Surface Coating	FR(τα)n	FRUC (W/m²·K)	Key Features
Type A	1	Standard black paint	0.74	6.58	Basic design, high heat loss, and lowest solar fraction performance

Type B	1	Black selective coating	0.74	5.10	Improved absorption, reduced emissivity, moderate performance
Type C	2	Standard black paint	0.684	4.02	Enhanced insulation, but absorber not optimized for selective absorption
Type D	2	Black selective coating	0.684	2.89	Best thermal performance, lowest heat loss, highest solar fraction

The standard efficiency test chart for the four types of solar collectors employed was used to get each coefficient's value $F_R U_C$, and $F_R(\tau\alpha)_n$, [35,36] F_R stands for the collector's heat removal factor, τ for the transmissivity of the transparent cover, and α for the absorber plate's absorption. In Table 3, can see the values of every collector.

Table 3. Value of $F_R U_C$ and $F_R(\tau\alpha)_n$ for the solar collectors used [37,30].

Coefficient	Collector Types			
	Type A	Type B	Type C	Type D
$F_R U_C$	6.58 W/K	5.10 W/K	4.02 W/K	2.89 W/K
$F_R(\tau\alpha)_n$	0.74	0.74	0.684	0.684

3. Results and discussion

The quantitative findings of this study are laid forth in great detail. For the five summer months (May–September), it utilized the MATHLAP software to solve the system mathematical model described in paragraph 3. It used four distinct varieties of solar collectors: type A, a black collector with a single cover; type B, a selective absorber collector with a single cover; type C, a black collector with two covers; and type D, a selective absorber solar collector with two covers. Because of this, there were able to calculate the values of the solar fraction factor (f) for the suggested system. The values of the ambient temperature ($\overline{T}_a$), the intensity of the solar radiation on the horizontal surface ($\overline{H}$), and the clearness index ($\overline{K}_T$) during the months in which the computation was conducted are shown in Table 1 for the city of Baghdad (Iraq).

3.1. The effect of solar storage capacity on solar fraction factor

Figures (2) illustrates the variation of solar fraction factor (f) with different values of storage capacity ranged between 25 - 125 kg of water per square meter of collector area, for four different types of solar collector (Type: A, B, C, and D), for one collection area (80) m2, and during 5 months of cooling season between May and September at Baghdad city / IRAQ. In all of these Figures, it is noted that increasing the storage capacity leads to a slight increase in the solar fraction. The increase in storage capacity (MS) can be attributed, according to the mathematical modeling of the Utilization, f-chart method (mentioned in section 2-2), to an increase in the value of the parameter a, which in turn leads to an increase in the useful energy gain (Qu) as shown in Eqn. (27). On the other hand, the increase in storage capacity also leads to an increase in the size of the solar collection tank, which in turn can cause an increase in the amount of heat loss from the tank to the surrounding environment. Therefore, the designer of the solar system must take care to choose the size of the solar collection tank to the extent that the heat loss from the tank does not become so large that it covers the benefit of increasing storage capacity. In addition, the Figure shows that the highest values of solar fraction were obtained from the solar collector type D, while the lowest values were obtained from the solar collector type A. The average values of solar fraction in this study were obtained from solar collector types B and C. In a solar collector, the transparent cover (glass cover) is used to reduce the convection losses from the absorber plate through the restraint of the stagnation air layer between the absorber plate and the glass. It also reduces the radiation losses from the collector because the spectral transmissivity of glass is such that it is transparent to short-wave radiation emitted by the sun and reflected by the sky, but nearly opaque to long-wave thermal radiation emitted by the interior of the collector. When two or more transparent covers are used, the radiation-convection losses are further reduced, as there are more surfaces to impede radiation and more stagnant air layers to impede convection. Radiation losses from the absorber of the solar collector can also be decreased significantly when the receiving surface has selective properties. Selective surfaces have height absorptivity for radiation in the

solar range of wavelengths and low emissivity for long-wave thermal radiation. The Figure also shows that the highest values of solar fraction (f) were obtained during September.

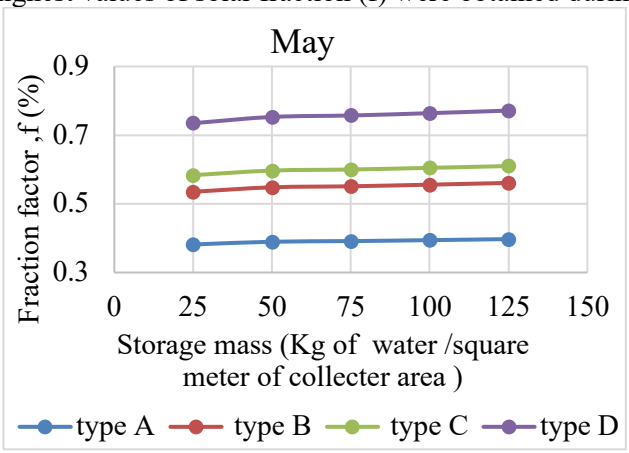

a. Fraction Factor with Storage Capacityin May, Ac =80m^2

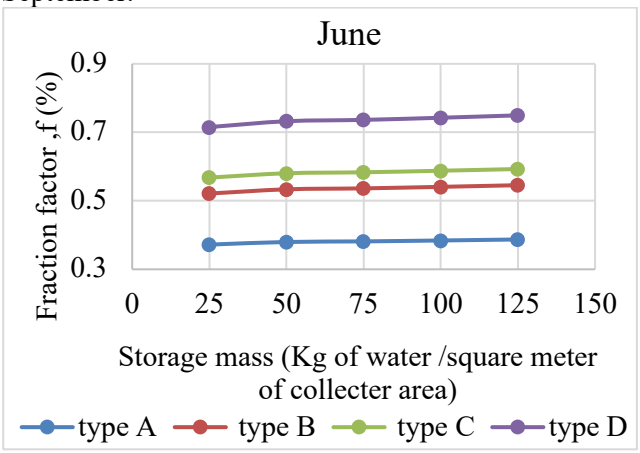

b. Fraction Factor with Storage Capacity in June, Ac = 80m^2

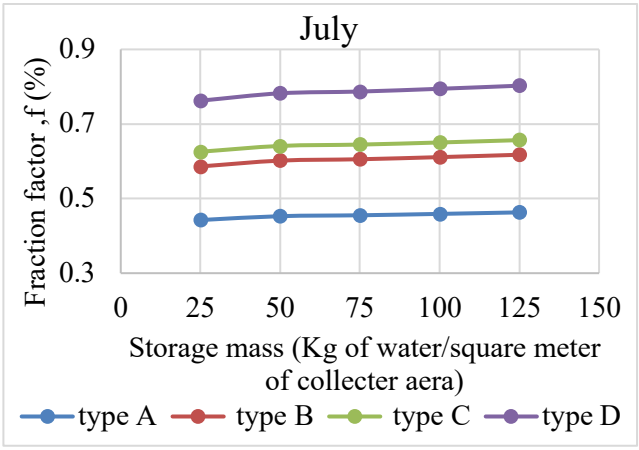

c. Fraction Factor with Storage Capacity in July, Ac = 80m^2

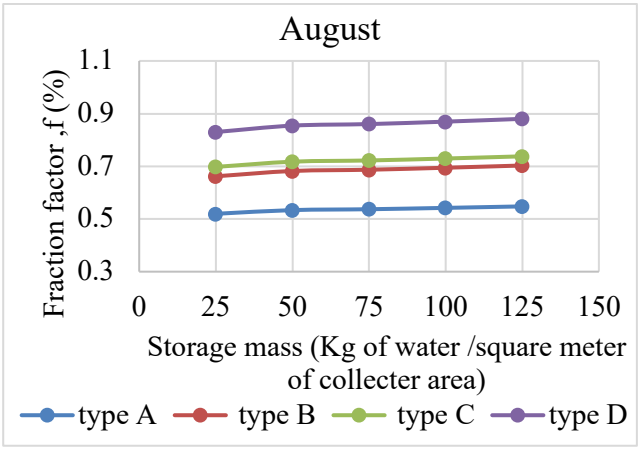

d. Fraction Factor with Storage Capacity in August, Ac = 80 m^2

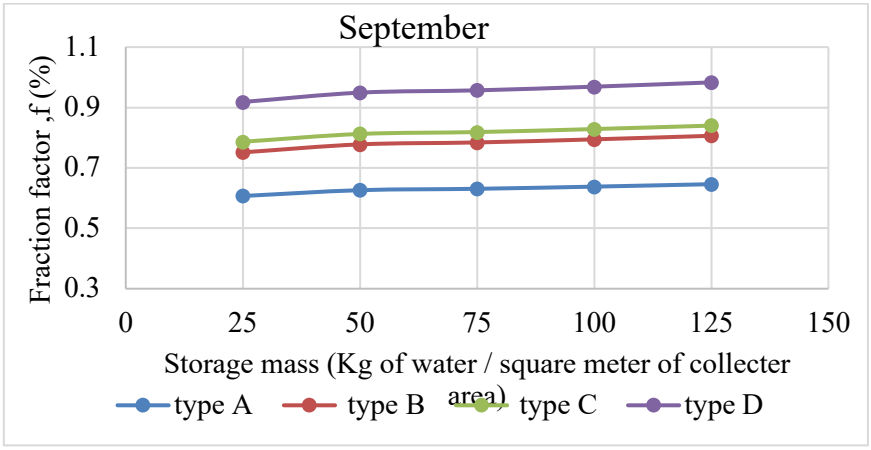

e. Fraction Factor with Storage Capacity in September, Ac = 80 m^2.

Figure 2. Fraction Factor with Storage Capacity for Different Types of Collectors at Different Months.

3.2. The effect of collector surface area on solar fraction factor

Figures (3) show the relation between collector area (AC) and the solar fraction factor (f) for four solar collectors used, for one mass of water in the storage tank MS (75 kg of water/m2 of collector area, and for five months of the summer season. Drawing the relationship between the solar collecting area and the solar fraction factor is a very useful tool that can be placed in the hands of the designer of the solar system through which, and

according to the economic criteria, a correct decision can be taken with regard to the required size of the system for a specific application. So, the designer can choose between designing a large-sized solar system with large collecting area and little dependence on the auxiliary system (that work on conventional fuel) or designing a solar system of a small size with great dependence on the auxiliary system or any other design that meet the economic consideration.

It is noted in all the aforementioned figures, that the solar fraction factor (f) of the solar system increases in approximately linear relation with the increase of solar collector area. By referring to the mathematical model for determining the thermal performance of the solar system and calculating the solar fraction factor for this system, it is noted that the solar collector area (AC) interfere with the calculation of the parameter X (equation 28), an increase in collecting area leads to an increase in the value of this parameter and thus ultimately increasing both the rate of useful gained energy (equation 27) and finally the solar fraction factor.

In addition, the Figures show that the highest values of solar fraction factor were obtained from the solar collector type D while the lowest values were obtained from the solar collector type A. The average values of solar fraction in this study were obtained from solar collector types B and C.

The figure also shows that increasing the collector area to a reasonable limits) slightly larger than 100 square meter) especially with solar collector type D, to reaching the values of f, during the months of peak solar radiation, equal to one. This meaning that the solar system in this case will be able to supply the full heat load required to the absorption machine operated by this system.

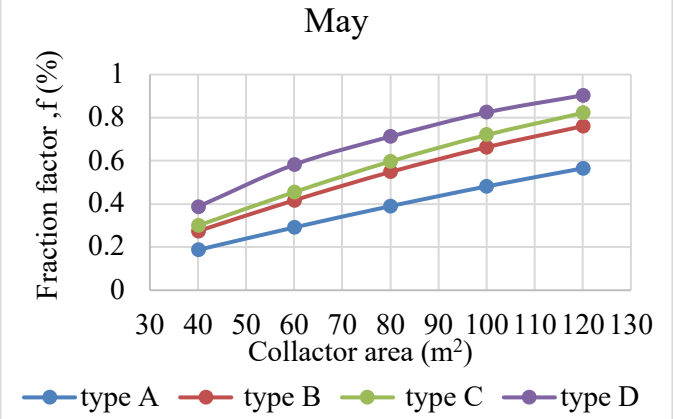

a. Fraction Factor with Collector Area in May, Storage Capacity M_S = 75 kg of Water/m^2 Collector Area.

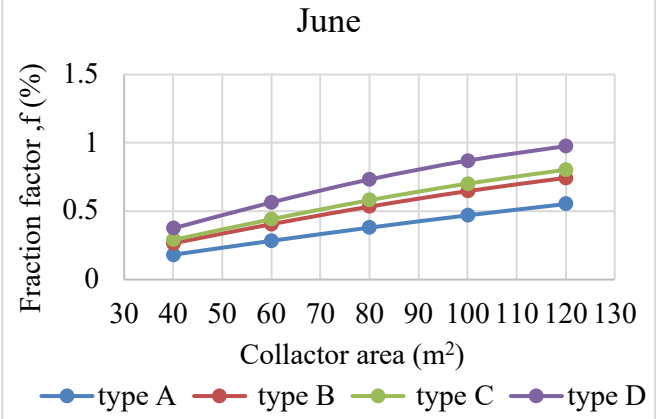

b. Fraction Factor with Collector Area in June, Storage Capacity M_S = 75 kg of Water/m^2 Collector Area.

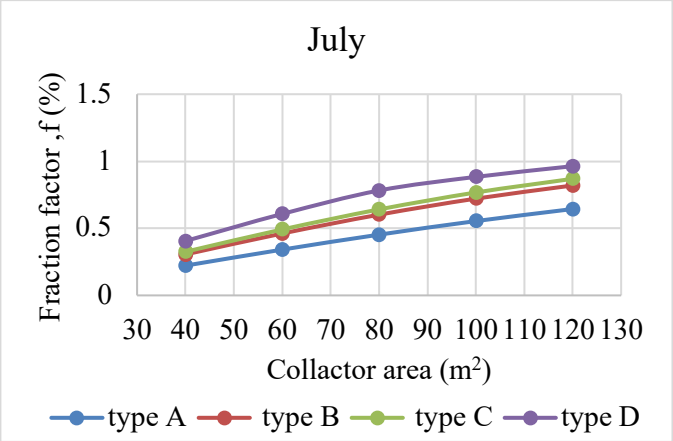

c. Fraction Factor with Collector Area in July, Storage Capacity M_S = 75 kg of Water/m^2 Collector Area.

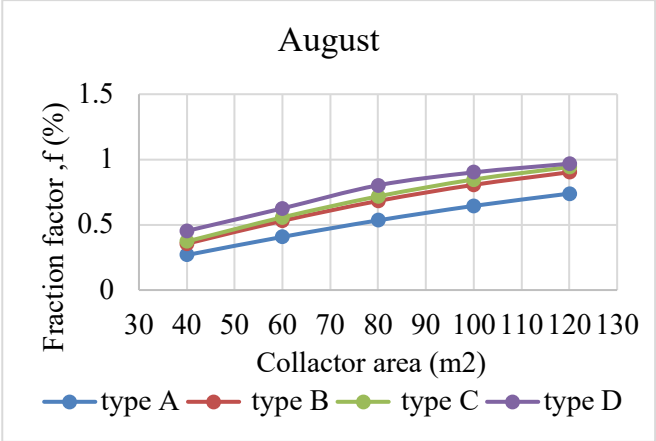

d.Fraction Factor with Collector Area in August, Storage Capacity M_S = 75 kg of Water/m^2 Collector Area.

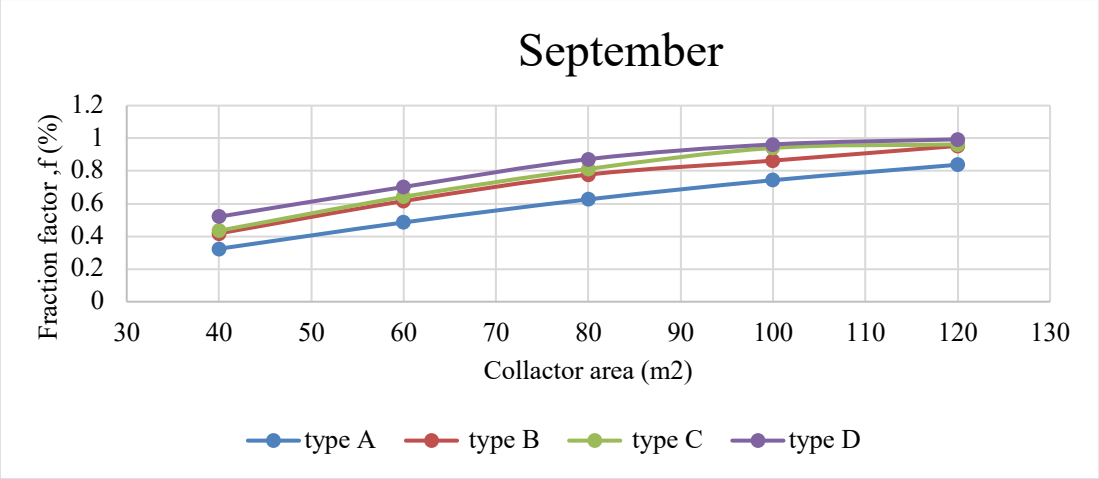

e. Fraction Factor with Collector Area of in September, Storage Capacity M_S =75 kg of Water/m^2 Collector Area.

Figure 3. Fraction Factor with Collector Area of Different Types of System different months, Storage Capacity M_S =75 kg of Water/m^2 Collector Area.

3.3. The effect of weather conditions in the months of the year on solar fraction

Table 4 presents the solar fraction factor (f) values for several types of collectors (A, B, C, and D) during the summer months from May to September. The analysis utilized an 80 m² solar collector area with a storage capacity of 75 kg/m². In September, the most efficient solar collector was type D, which featured a specialized absorbing surface and two transparent covers, achieving a solar fraction factor of 0.94928. Conversely, the type A collector, with a single transparent cover and a conventional black absorbing surface, displayed the lowest performance, recording a solar fraction factor of 0.37829 in May. Meanwhile, types B and C collectors exhibited moderate performance, with solar fraction factor values ranging from 0.53305 for type B in May to 0.81246 for type C in September. According to Table 1, the decrease in ambient temperature during September contributes to the noticeable increase in solar fraction factors for that month. Lower ambient temperatures reduce the system's thermal load and decrease the collector's inlet fluid temperature. However, the fluid in the storage tank or connecting pipes may lose some heat due to heat exchange with the cooler surrounding air, leading to a drop in temperature before reaching the solar collector. Consequently, solar collectors operate more efficiently under these conditions.

Table 4. Solar Fraction Factor of Different Types of Collectors with the Collector Area 80m^2, Storage Capacity 75kg/m^2 Collecting Area.

Months	Solar fraction factor(f)			
	Type A	Type B	Type C	Type D
May	0.37829	0.53305	0.58056	0.73368
June	0.37976	0.53351	0.58040	0.73232
July	0.43997	0.58574	0.62404	0.76263
August	0.51916	0.66503	0.69940	0.83434
September	0.62626	0.77794	0.81246	0.94928

The excellent performance of Type D collectors, having two transparent covers and a selective black absorber surface as an example[38], has highlighted that selective coated solar collector and a double-glazed solar collector can considerably lower both the radiative and convective losses and thus improve on the thermal efficiency when the solar radiation is high. On the same note,[39] flat-plate collectors could attain a solar utilizeability of over 0.90 with the application of selective surfaces and optimal tilt angles. As it can be seen in the current study, the solar fraction factor of Type D collectors in September was 0.949, matching the values obtained , who optimized large-area systems with simulation-based optimization to achieve maximum solar

fractions of up to 0.94. These findings[38] validate the f-chart method as a tool of preliminary design and demonstrate that the closed-loop system with Type D collectors works on the high-performance side of reported performance bands in similar climatic regions. In comparison, Type A collectors, without selective coatings and having a single cover, rated as low as 0.378 solar fraction, confirming the literature conclusion that the traditional absorber design is inadequate to high-efficiency operation in hot-climate environments. Thus, this research both confirms earlier results, but also shows that large performance improvements can be obtained by fairly modest improvements in collector design - particularly when combined with such tools as the f-chart approach to early-stage system sizing.

4. Conclusion

This research has highlighted the importance of solar water heating systems in supporting the thermal energy requirements of absorption refrigeration units, especially in hot, dry climates such as Baghdad, Iraq. In this case the results of this study identify, rather than repeating technical results, the following valuable perspectives for the design and optimization of solar thermal systems in such regions:
Prioritize Collector Efficacy High-efficiency collectors (e.g. Type D with selective black coatings/double transparent covers) have consistently demonstrated higher thermal performance. By reducing radiative and convective heat losses, high-performance collectors will maximize solar energy usage, where solar radiation is at its greatest. Increasing System Size through Collector Area is More Effective than Increasing Storage Volume While storage capacity is beneficial for stabilizing performance, the results suggest that increasing the surface area of the collectors is a more effective strategy for increasing the solar fraction. Again, this makes the original sizing of the collector, early in the design process, very important. The f-Chart Method is a Useful Design Tool The near perfect fit between simulated results and expected ranges confirms that the f-chart method is useful for initial system sizing. In practical terms, it allows designers to make reasonable performance predictions and adjust parameters. Implications on Future Systems Being Designed for Arid Regions For communities with weather patterns similar to Baghdad, acquiring advanced collector technologies and better sizing techniques can allow for nearly complete operation with solar energy during peak loads in summer. Overall, this will reduce grid dependency while creating sustainable cooling options for this hot climate.

Declaration of Competing Interest

The authors declare that there are no conflicts of interest regarding the publication of this manuscript.

Funding Information

No funding was received from any financial organization to conduct this research.

Author Contributions

All authors proposed the research problem. Author Fatima Hilal Abish collected recent articles and organized them in simple shapes. Authors Fatima Hilal Abish and Abdulsalam D.M. Hassen verified the recommendation in the proposed work. Author Fatima Hilal Abish designed and proposed the work. Authors Fatima Hilal Abish and Abdulsalam D.M. Hassen discussed the proposed design. All the authors discussed the results and the final version of this paper.

References

[1] P. Charoensawan, P. Wilaipon, and N. Seehawong, “Flat Plate Solar Water Heater With Closed-Loop Oscillating Heat Pipes,” Thermal Science, vol. 25, no. 5, pp. 3607–3614, 2021, doi: 10.2298/TSCI200713192C.

[2] Vishal Singh and Vishwajeet Kureel, “Performance Optimization of Solar Water Heating Systems in Different Climates,” International Journal of Modern Engineering & Management Research, vol. 12, no. 3, 2024, Accessed: Jul. 27, 2025. [Online]. Available: https://www.ijmemr.org/Publication/V12I3/IJMEMR-V12I3-002.pdf

[3] A. Herez et al., “Solar water heating: comprehensive review, critical analysis and case study,” International Journal of Thermofluids, vol. 20, Nov. 2023, doi: 10.1016/j.ijft.2023.100503.

[4] H. Fayaz, N. A. Rahim, R. Saidur, and M. Hasanuzzaman, "Techno-economic Analysis of Evacuated Tube Solar Water Heater using F-chart Method," in IOP Conference Series: Materials Science and Engineering, Institute of Physics Publishing, May 2018. doi: 10.1088/1757-899X/358/1/012016.

[5] Kerme and Kaneesamkandi, "Performance analysis and design of liquid based solar heating system," vol. 1, no. 1, pp. 182–191, Feb. 2015, doi: https://doi.org/10.18186/jte.02359.

[6] M. Tunç and Ü. Çamdalı, "Optimal Domestic Solar Space and Water Heating System in Çeşme," INTERNATIONAL JOURNAL of RENEWABLE ENERGY RESEARCH M. Tunc and U. Camdali, vol. 7, no. 4, Nov. 2017, [Online]. Available: www.enerji.gov.tr

[7] M. Gojak, F. Ljubinac, and M. Banjac, "Simulation of solar water heating system," FME Transactions, vol. 47, no. 1, pp. 1–6, 2019, doi: 10.5937/fmet1901001G.

[8] S. Sirdaş, "Daily wind speed harmonic analysis for Marmara region in Turkey," Energy Convers Manag, vol. 46, no. 7, pp. 1267–1277, 2005, doi: https://doi.org/10.1016/j.enconman.2004.06.020.

[9] S. A. Klein, W. A. Beckman, and J. A. Duffie, "A design procedure for solar heating systems," Solar Energy, vol. 18, no. 2, pp. 113–127, 1976, doi: https://doi.org/10.1016/0038-092X(76)90044-X.

[10] J. G. Cardoso, I. R. S. Casella, A. J. S. Filho, F. F. Costa, and C. E. Capovilla, "SCIG wind turbine wireless controlled using morphological filtering for power quality enhancement," Renew Energy, vol. 92, pp. 303–311, 2016, doi: https://doi.org/10.1016/j.renene.2016.02.014.

[11] A. Mehmeti, J. Pedro Pérez-Trujillo, F. Elizalde-Blancas, A. Angelis-Dimakis, and S. J. McPhail, "Exergetic, environmental and economic sustainability assessment of stationary Molten Carbonate Fuel Cells," Energy Convers Manag, vol. 168, pp. 276–287, 2018, doi: https://doi.org/10.1016/j.enconman.2018.04.095.

[12] M. Adouane, A. Al-Qattan, B. Alabdulrazzaq, and A. Fakhraldeen, "Comparative performance evaluation of different photovoltaic modules technologies under Kuwait harsh climatic conditions," Energy Reports, vol. 6, pp. 2689–2696, 2020, doi: https://doi.org/10.1016/j.egyr.2020.09.034.

[13] K. Sangeetha, A. S. Liz, P. Suganthi, and D. L. Femilinjana, "Integrating Machine Learning Algorithms for Predicting Solar Power Generation," in E3S Web of Conferences, EDP Sciences, May 2023. doi: 10.1051/e3sconf/202338701004.

[14] G. Ruan, J. Wu, H. Zhong, Q. Xia, and L. Xie, "Quantitative assessment of U.S. bulk power systems and market operations during the COVID-19 pandemic," Appl Energy, vol. 286, p. 116354, 2021, doi: https://doi.org/10.1016/j.apenergy.2020.116354.

[15] S.-Y. Wu, L. Xu, and L. Xiao, "Air purification and thermal performance of photocatalytic-Trombe wall based on multiple physical fields coupling," Renew Energy, vol. 148, pp. 338–348, 2020, doi: https://doi.org/10.1016/j.renene.2019.10.039.

[16] P. Si, Y. Lv, X. Rong, L. Shi, J. Yan, and X. Wang, "An innovative building envelope with variable thermal performance for passive heating systems," Appl Energy, vol. 269, p. 115175, 2020, doi: https://doi.org/10.1016/j.apenergy.2020.115175.

[17] R. R. Rustum and A. D. Al-Nadawi, "Using the utility method - F-scheme in studying the long-term thermal performance of the heat-storage and transmitting wall (Trombe wall)," Wasit Journal of Engineering Sciences, vol. 10, no. 2, pp. 69–82, Jun. 2022, doi: 10.31185/ejuow.Vol10.Iss2.261.

[18] R. Alayi, N. Khalilpoor, S. Heshmati, A. Najafi, and A. Issakhov, "Thermal and Environmental Analysis Solar Water Heater System for Residential Buildings," International Journal of Photoenergy, vol. 2021, 2021, doi: 10.1155/2021/6838138.

[19] J. D. Gil, A. Topa, J. D. Álvarez, J. L. Torres, and M. Pérez, "A review from design to control of solar systems for supplying heat in industrial process applications," Jul. 01, 2022, Elsevier Ltd. doi: 10.1016/j.rser.2022.112461.

[20] D. Huang et al., "Study on the Energy Efficiency Improvement and Operation Optimization of a Solar Water Heating System," Applied Sciences (Switzerland), vol. 12, no. 14, Jul. 2022, doi: 10.3390/app12147263.

[21] A. Whillier, "Solar energy collection and its utilization for house heating (Sc.D. Thesis). Massachusetts Institute of Technology". Retrieved from MIT Digital Repository," 1963.

[22] B. Y. H. Liu and R. C. Jordan, "The long-term average performance of flat-plate solar-energy collectors: With design data for the U.S., its outlying possessions and Canada," Solar Energy, vol. 7, no. 2, pp. 53–74, 1963, doi: https://doi.org/10.1016/0038-092X(63)90006-9.

[23] M. Zlateva, "Assessment of the annual performance of solar collectors by means of the utilizability method," in E3S Web of Conferences, EDP Sciences, Nov. 2020. doi: 10.1051/e3sconf/202020702007.

[24] M. Collares-Pereira and A. Rabl, “The average distribution of solar radiation-correlations between diffuse and hemispherical and between daily and hourly insolation values,” Solar Energy, vol. 22, no. 2, pp. 155–164, 1979, doi: https://doi.org/10.1016/0038-092X(79)90100-2.
[25] S. A. Klein and W. A. Beckman, “A general design method for closed-loop solar energy systems,” Solar Energy, vol. 22, no. 3, pp. 269–282, 1979, doi: https://doi.org/10.1016/0038-092X(79)90142-7.
[26] M. D.-E. Sarmouk, A. Smaili, H. Fellouah, and A. Merabtine, “Experimental and numerical investigations of a solar space heating system based on design of experiments method,” Solar Energy, vol. 216, pp. 396–410, 2021, doi: https://doi.org/10.1016/j.solener.2021.01.039.
[27] D. Marano, V. Sabatelli, and G. Fiorenza, “Techno-Economic Evaluation of Solar-Assisted Air-Conditioning Systems in Europe,” 2007. [Online]. Available: https://www.researchgate.net/publication/357631813
[28] I. S. Marinopoulos and K. L. Katsifarakis, “Optimization of Energy and Water Management of Swimming Pools. A Case Study in Thessaloniki, Greece,” Procedia Environ Sci, vol. 38, pp. 773–780, 2017, doi: 10.1016/j.proenv.2017.03.161.
[29] L. Enriquez, J. Gabriel, D. Casas, and S. Isabel, “USABILIDAD EN APLICACIONES MÓVILES.”
[30] S. A. Klein, “Calculation of flat-plate collector utilizability,” Solar Energy, vol. 21, no. 5, pp. 393–402, 1978, doi: https://doi.org/10.1016/0038-092X(78)90171-8.
[31] J. C. Mitchell, J. C. Theilacker, and S. A. Klein, “Calculation of monhly average collector operating time and parasitic energy requirements,” Solar Energy, vol. 26, no. 6, pp. 555–558, 1981, doi: https://doi.org/10.1016/0038-092X(81)90169-9.
[32] E. M. Ismail, S. J. Flayh, M. Saeedmohammed, and K. S. Mohammed, “Heat Exchanger Design and Optimization for Industrial Applications,” Nanotechnol Percept, vol. 20, no. S3, pp. 211–229, 2024, doi: doi:10.62441/nano-ntp.v20is3.18.
[33] A. K. Alshara, A. Mohsin Alsayah, M. Saeed Mohammed, S. Fahad Dakel, and A. Kadhim Alshara, “Numerical and experimental study of heat transfer in shell-and U-tube heat exchanger with baffles,” Chinese Journal of Geotechnical Engineering, vol. 44, no. 5, Jan. 2022, doi: 10.11779/CJGE202205.2.
[34] L. Caretto, “The f-Chart Method for Solar Chart Method for Solar Collectors Collectors Alternative Energy Alternative Energy,” 2010. [Online]. Available: http://www.fchart.com/
[35] S. A. Kalogirou, “Solar thermal collectors and applications,” Prog Energy Combust Sci, vol. 30, no. 3, pp. 231–295, 2004, doi: https://doi.org/10.1016/j.pecs.2004.02.001.
[36] Ashrae standard, “Methods of Testing to Determine the Thermal Performance of Solar Collector,” American society of heating, Refrigerating and Air-Conditioning Engineers, 1977.
[37] M. R. Clot, P. Rosa-Clot, and G. M. Tina, “Submerged PV Solar Panel for Swimming Pools: SP3,” in Energy Procedia, Elsevier Ltd, 2017, pp. 567–576. doi: 10.1016/j.egypro.2017.09.565.
[38] T. Echániz, I. Setién-Fernández, R. B. Pérez-Sáez, C. Prieto, R. E. Galindo, and M. J. Tello, “Importance of the spectral emissivity measurements at working temperature to determine the efficiency of a solar selective coating,” Solar Energy Materials and Solar Cells, vol. 140, pp. 249–252, Sep. 2015, doi: 10.1016/j.solmat.2015.04.009.
[39] B. A. Ternenge, Zwalnan. J. S, N. N. Caleb, and E. E. Oguche, “Flat Plate Solar Collectors for Process Heat: A Review,” International Journal of Research Publication and Reviews, vol. 2, no. 8, pp. 1402–1407, 2021, [Online]. Available: www.ijrpr.com